1
2 **Bristlecone Pine Maximum Latewood Density as a Superior Proxy for Millennium-length Temperature Reconstructions**

3 **T. De Mil[1,†], V. Matskovsky[2,3,†], M. Salzer[4], L. Corluy[2,3], L. Verschuren[2,3], C. Pearson[4], L.**
4 **Van Hoorebeke[3], V. Trouet[4,5] and J. Van den Bulcke[2,3]**

5 [1] Forest Is Life, TERRA Teaching and Research Centre, Gembloux Agro Bio-Tech, University
6 of Liège, Passage des Déportés 2, B-5030, Gembloux, Belgium.

7 [2] UGent-Woodlab, Laboratory of Wood Technology, Department of Environment, Ghent
8 University, Coupure Links 653, B-9000, Gent, Belgium.

9 [3] UGent Centre for X-ray Tomography (UGCT), Proeftuinstraat 86, B-9000, Gent, Belgium.

10 [4] Laboratory of Tree-Ring Research, University of Arizona, 1215 E Lowell St, Tucson, AZ,
11 85721, United States.

12 [5] Belgian Climate Centre, Uccle, Belgium.

13 † These authors contributed equally to this work

14 Corresponding author: Tom De Mil (tom.demil@uliege.be)

15 **Key Points:**

16 • We present the first X-ray Computed Tomography-derived MXD-based temperature
17 reconstruction using Bristlecone pine tree cores.
18 • Bristlecone pine maximum latewood density is a reliable proxy for warm-season
19 temperature over a large part of the American Southwest.
20 • Our reconstruction (1625 – 2005 CE) contains low-frequency variability and can be
21 prolonged over a large part of the Holocene

22

23 **Abstract**

24 Bristlecone pine (*Pinus longaeva*) (PILO) trees exhibit exceptional longevity. Their tree-ring
25 width (TRW) series offer valuable insights into climatic variability. Maximum latewood density
26 (MXD) typically correlates better with temperature variations than TRW, yet PILO MXD
27 records are non-existent due to methodological challenges related to their tree-ring structure.
28 Here, we used an X-ray Computed Tomography (X-ray CT) toolchain on 51 PILO cores from
29 the California White Mountains to build a chronology that correlates significantly (r=0.66,
30 p<0.01) with warm-season (March-September) temperature over a large spatial extent. This led
31 to the first X-ray CT-based temperature reconstruction (1625 – 2005 CE). Good reconstruction
32 skill (RE=0.51, CE=0.32) shows that extending MXD records across the full length of the PILO
33 archive could yield a robust warm-season temperature proxy for the American Southwest over
34 millennia. This breakthrough opens avenues for measuring MXD in other challenging conifers,
35 increasing our understanding of past climate further, particularly in lower latitudes.

36

37 **Plain Language Summary**
38 The ancient Bristlecone pine trees can live for several millennia and hold invaluable climate
39 information. Their annual rings were used to develop millennium-length records of the Holocene
40 climate. Maximum latewood density (MXD), which is the highest wood density value in the
41 latewood of a tree ring, has been shown to closely follow summer temperature in different
42 conifer species, but not yet in Bristlecone pine. The gnarly and twisted growth of these ancient
43 trees has presented significant hurdles for MXD analysis. Here we apply an X-ray Computed
44 Tomography toolchain that allows us to 3D scan through the tissue of a tree ring and to map
45 MXD variations. Using this new technique, we were able to reconstruct warm-season
46 temperature for the American Southwest back to 1625 CE. With these findings, we are confident
47 that a full-length reconstruction (back to 2575 BCE) can yield the longest annually resolved
48 temperature construction for this continent.

49 **1 Introduction**

50   Our understanding of temperature variability in the American Southwest over the past
51 centuries to millennia is incomplete (King et al., 2024; Trouet et al., 2013; Wahl et al., 2022).
52 Climatologically speaking, this region is important because of its sensitivity to variability in the
53 El Niño Southern Oscillation (ENSO) system (Cayan et al., 1999) and in the Hadley Circulation
54 (Alfaro-Sánchez et al., 2018). Furthermore, the region is characterized by the past occurrence of
55 mega-droughts and, multi-decadal dry periods with profound impacts on ecosystems and human
56 systems (Cook et al., 2004; Williams et al., 2020). In contrast to hydroclimate, the temperature
57 history of the American Southwest is less well understood (King et al., 2024). The most highly
58 resolved and precisely dated records of past climate over the Holocene are derived from tree-ring
59 series (Ahmed et al., 2013; Emile-Geay et al., 2017; Esper et al., 2012). For the American
60 Southwest, millennial-length tree-ring chronologies that extend deep into the Holocene are
61 limited to Bristlecone pine (*Pinus longaeva* D.K. Bailey, PILO) records (Salzer et al., 2019).
62 Lower forest border sites such as the iconic Methuselah Walk site (Ferguson, 1968), of which the
63 chronology was recently updated to 8349 BCE (Salzer et al., 2019), provide an accurate
64 estimation of past precipitation variability, but lack a strong temperature signal. Samples from
65 upper treeline sites in the same region have been shown to carry a temperature signal
66 (Kipfmueller & Salzer, 2010; LaMarche & Stockton, 1974; Salzer et al., 2009). Salzer et al.

67   (2014) developed a tree-ring width (TRW)-based temperature reconstruction (2575 BCE – 2006
68   CE) based on living and dead upper treeline PILO trees. However, the temperature signal in this
69   TRW record is limited to carefully selected trees growing near the very upper treeline (Salzer et
70   al., 2014) and is best expressed at (multi-) decadal time scales, rather than annual scales. PILO
71   TRW variability is also influenced by memory effects and by subtle micro-topographical effects
72   (Bruening et al., 2017; Bunn et al., 2011; Tran et al., 2017), which makes an annually resolved
73   temperature reconstruction from the PILO TRW archive challenging. At both high latitudes
74   (Briffa et al., 1988; Esper et al., 2018) and mid latitudes (Büntgen et al., 2010; Klippel et al.,
75   2020; Trouet et al., 2012), maximum latewood density (MXD) has shown to be a better proxy for
76   summer temperature than TRW. MXD captures the temperature signal as follows: at the end of
77   the growing season, smaller and thicker-walled latewood cells are formed (Rathgeber, 2017).
78   Growing season temperatures affect the duration of the cell-wall thickening process, which
79   results in MXD variations (i.e. warmer temperatures generate higher MXD values).

80   However, the International Tree-Ring Data Bank (ITRDB) only holds 575 sets of MXD data
81   compared to over 4200 sets of TRW data (St. George & Esper, 2019; Zhao et al., 2019). MXD
82   chronologies from low-latitude and semi-arid regions are even more rare. Hence, there is a need
83   to both update and extend MXD chronologies (St. George & Esper, 2019). The main limitation
84   of MXD is the restricted availability of the necessary measurement equipment and its time-
85   consuming nature compared to TRW: fewer than a dozen facilities exist worldwide that conduct
86   conventional X-ray densitometry. Moreover, conventional MXD facilities use measuring
87   equipment that requires the X-ray beams to be parallel to the tracheids (Schweingruber et al.,
88   1978). This has prohibited MXD measurements on PILO samples due to the twisted tracheid
89   angle of the wood, illustrated by its gnarly growth shape (Figure 1a). Nevertheless, PILO records
90   have the potential to drastically extend the current temporal extent of MXD data, which reaches
91   back to 138 BCE (Esper et al., 2012). X-ray Computed Tomography (X-ray CT) has emerged as
92   a valuable tool for deriving TRW and density variables from challenging wood samples (Van
93   den Bulcke et al., 2014; De Mil et al., 2016). It can be used to correct for grain angle, thus
94   overcoming tedious laboratory steps and allowing to extract information from deformed tissues
95   (De Mil et al. 2017). X-ray CT has shown its reliability for generating accurate MXD values
96   (Björklund et al., 2019; Bytebier et al., 2022; De Mil et al., 2021).

97   Here, we apply X-ray CT to PILO samples from the California White Mountains and present the
98   first ever X-ray CT based MXD temperature reconstruction. To achieve this, we (i) measure
99   MXD with X-ray CT, (ii) examine the strength of the signal and spatiotemporal stability of the
100 MXD- temperature correlation, and (iii) assess skill and compare our reconstruction with other
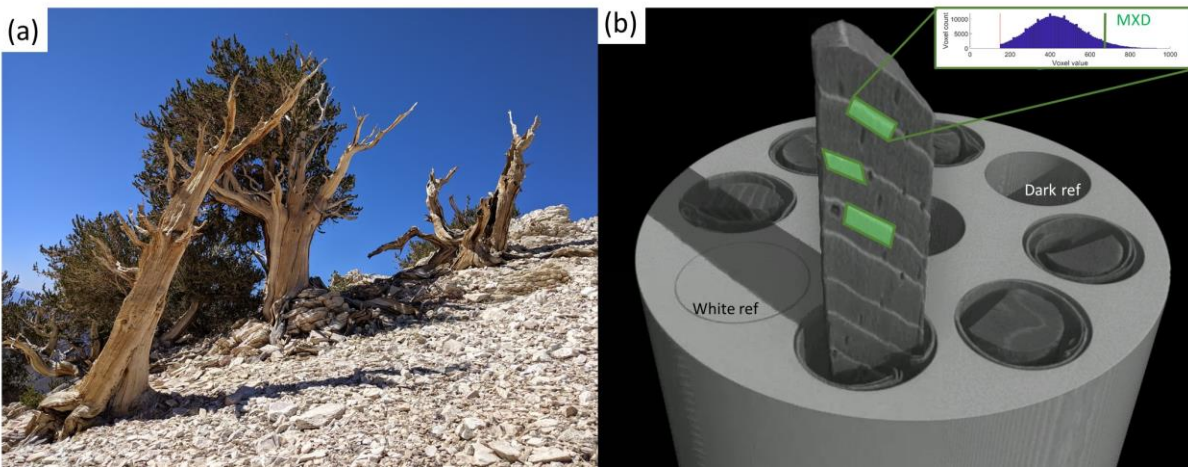101 local and regional temperature reconstructions.

102 **2 Materials and Methods**

103   2.1 Scanning and processing of tree-ring cores

104 We selected 51 mounted and dated PILO cores from the collection of the Laboratory of Tree-
105 Ring Research (University of Arizona) originating from the California White Mountains site
106 (Figure 1a) (37.57N 118.21W - 37.51N 118.17W). The site contains the following treeline
107 microsites: (i) Sheep Mountain (SHP) (3395 – 3501 m ASL) (24 cores from 23 trees from a field
108 mission in September 2005), (ii) South Face (SF) (3445-3480 m ASL) (14 cores from 9 trees
109 sampled in September 2009), and (iii) Cottonwood Upper (CWU) (3470-3512 m ASL) (13 cores

110 from 10 trees from a field mission in September 2014). Initial pre-selection was based on
111 previous TRW dating, avoiding cores with many missing rings. We unmounted the cores, placed
112 them into paper straws and refluxed in a Soxhlet apparatus for 24h in an ethanol/toluene mixture,
113 followed by a 24h hot water bath.
114 We used the X-ray CT toolchain (De Mil & Van den Bulcke, 2023) to process the dried and
115 conditioned cores. We scanned the cores at 15 μm approximate volume pixel (voxel) pitch
116 (further referred to as resolution) (70 kV, 20W, 180ms, source detector distance 540 mm, source
117 object distance 54 mm, 4250 projections per full rotation) using a helical scanning procedure
118 (Van den Bulcke et al., 2014) with the CoreTOM scanning system (TESCAN - XRE, Ghent,
119 Belgium). The resulting projections were then reconstructed to 3D volumes using Octopus
120 Reconstruction software (Vlassenbroeck et al., 2007). We then treated the 3D images with the X-
121 CT software (www.dendrochronomics.ugent.be (De Mil & Van den Bulcke, 2023)). We first
122 extracted 3D core volumes from the virtual sample holder (Figure 1b) and then calibrated the
123 volume with the reference material and air hole of the sample holder (De Ridder et al., 2011).
124

125
126
**Figure 1. The X-ray Computed Tomography (X-ray CT) toolchain. (a) The iconic
Bristlecone pine trees from the California White Mountains, with their gnarly and slow
growth hindering MXD measurements, (b) an X-ray CT 3D rendered image (created with
VGStudio Max from Volume Graphics) of a polymer sample holder with solvent-extracted
tree cores in paper straws. Black holes and filled holes are air and reference material
respectively to convert grey-value voxels into wood density values. An extracted core from
the sample holder is shown where subregions (green) containing the ring boundaries are
indicated, and where grain and ring angle are taken into account. The resulting MXD
values are calculated by retaining the 95th percentile of the values within this volume
(inset). Scanning resolution is 15 μm.**

138 We then indicated tree-ring boundaries using a graphical user interface (De Mil et al., 2016).
139 Small deviations in ring or grain angle can impact the density values (Björklund et al., 2019):
140 therefore, both the radial and transversal planes of the cores were corrected for ring and grain
141 deviations (Van den Bulcke et al., 2014). To avoid resin ducts or irregular ring boundaries
142 (indented rings), a subvolume was selected for every ring (Figure 1b). To calculate the MXD
143 value for each ring, we selected the 95th percentile of values from all the voxels from this
144 subvolume.

145 Finally, we checked our TRW series against crossdated TRW series for the same cores that were
146 previously measured with a Velmex system to 0.001 mm precision (Salzer et al., 2014) and
147 exported the MXD data for chronology development.

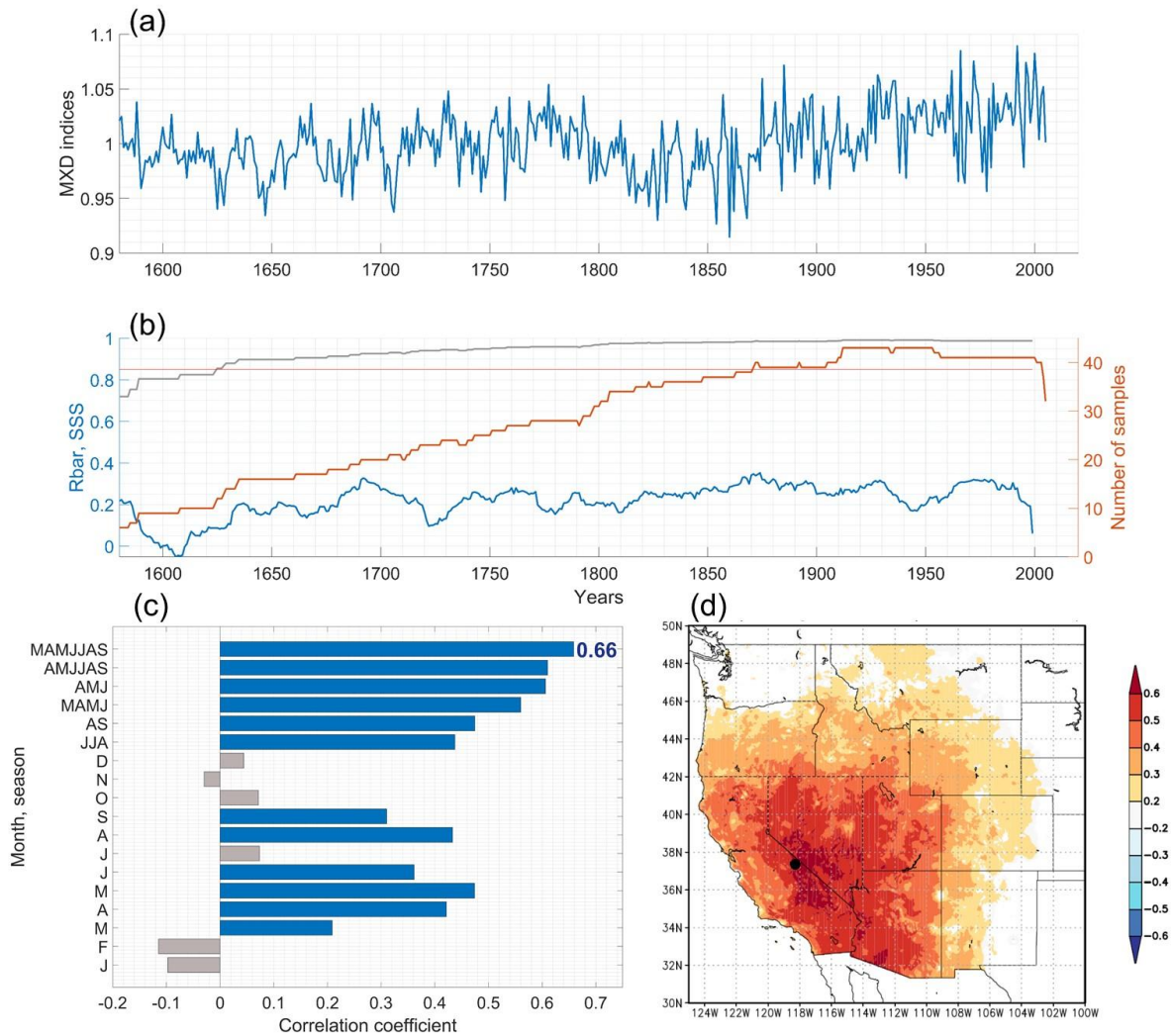148   2.2 Chronology development and climate data

149 We additionally checked crossdating of the obtained MXD series using COFECHA software
150 (Holmes, 1983). We used Dplr (Bunn, 2008, 2010) in the R programming environment (R Core
151 Team 2023) to assess the chronology statistics such as mean interseries correlation (RBAR) and
152 Subsample Signal Strength (SSS) (Wigley et al., 1984), as well as to detrend the series and for
153 chronology building. We tested various detrending options for the MXD data (Figure S1 in
154 Supporting Information S1) and decided to use an age-dependent spline with signal-free
155 implementation (Melvin & Briffa, 2008). Then, we used a bi-weight robust mean to average the
156 obtained dimensionless indices into the final MXD chronology based on 51 dated series with an
157 average length of 259 years and 13,202 measurements in total. We cut the resulting chronology
158 off in 2005, as sample replications drops rapidly thereafter. We extracted monthly mean air
159 temperature and monthly precipitation sums (1895-2005) from the Parameter-elevation
160 Relationships on Independent Slopes Model (PRISM) dataset (Daly et al., 2008) using a NetCDF
161 file with 0.25° spatial resolution from KNMI Climate Explorer (Trouet & Van Oldenborgh,
162 2013). The values were averaged over an area approximately 350 by 350 km (35.1875° -
163 38.1875° N; 119.1458° - 115.1458° W) to the east, north and south of the study area, roughly
164 corresponding to the region of the highest correlation between the developed MXD chronology
165 and the gridded mean temperature from PRISM dataset. We correlated our MXD chronology
166 (Pearson correlation coefficient) with monthly and seasonal mean climate data, both for the
167 whole period and with a 30-year sliding window. We then selected the seasonal temperature with
168 the strongest correlation with MXD as a reconstruction target. We fit a linear regression model to
169 predict the temperature with the MXD chronology as an independent variable.
170 To assess the skill of the reconstruction, we performed split calibration-validation tests for 1895-
171 1949 CE and 1950-2005 CE. We calculated correlation in the calibration (r_c) and validation (r_v)
172 periods, coefficient of determination in the calibration period (R^2_c), reduction of error (RE) and
173 coefficient of efficiency (CE) of the model (Cook et al., 1994). Then we used the full
174 instrumental period (1895-2005 CE) for the final calibration of the model.
175 We further generated field correlation maps between our MXD chronology and the PRISM
176 gridded temperature data using the KNMI climate explorer (Valerie Trouet & Van Oldenborgh,
177 2013).
178

179 **3 Results**

180   3.1 MXD chronology and temperature correlation

181 The generated MXD values have a mean value of 0.72 g·cm^{-3} and a standard deviation of 0.07
182 g·cm^{-3}. Mean RBAR and SSS of the resulting MXD chronology (Figure 2a) are 0.255 and 0.948
183 respectively (Figure 2b). A cut-off of SSS > 0.85 restricted our reconstruction to the earliest date
184 of 1625 CE. For this period, the mean signal-to-noise ratio is 18.12 and the first-order
185 autocorrelation is 0.41. PILO MXD is significantly (p<0.05) positively correlated with monthly
186 mean temperatures from current March to September, with a peak in May and a drop in
187 correlation below the significance level in July (Figure 2c). The strongest correlation coefficients

188   are obtained with the March-September (MAMJJAS) mean temperature ($r = 0.66$, $p < 0.01$). This
189   correlation is temporally stable, which is confirmed by performing a moving window (Figure S2
190   in Supporting Information S1). Correlation coefficients with precipitation were negative for most
191   months and less significant than for temperature (Figure S3 in Supporting Information S1).
192   Significant correlations of the PILO MXD record with temperature extend over a large part of
193   the American Southwest (Figure 2d). Correlation coefficients were high ($r > 0.6$, $p < 0.01$) over
194   the Sierra Nevada and the Great Basin and significant ($r > 0.4$, $p < 0.1$) over California, Nevada,
195   Arizona and Utah. Correlation coefficients decrease rapidly to the east of the Rocky Mountains
196   and to the north of the Great Basin, in the states of Oregon, Idaho, Wyoming, Colorado and New
197   Mexico (Figure 2d).

198

199   **Figure 2. The PILO MXD chronology, its statistics and correlation to climate variables. (a)**
200   **MXD chronology of PILO. (b) Sample size (orange curve), 30-year (with 15-year lag)**
201   **running SSS (grey curve) and RBAR (blue curve). Horizontal red line indicates the SSS =**
202   **0.85 threshold. (c) Pearson correlation coefficients between the MXD chronology and**
203   **monthly and seasonal PRISM mean temperature (Daly et al., 2008) for the period 1895-**
204   **2005 CE. Significant correlations are indicated in blue (p < 0.05), and the correlation value**
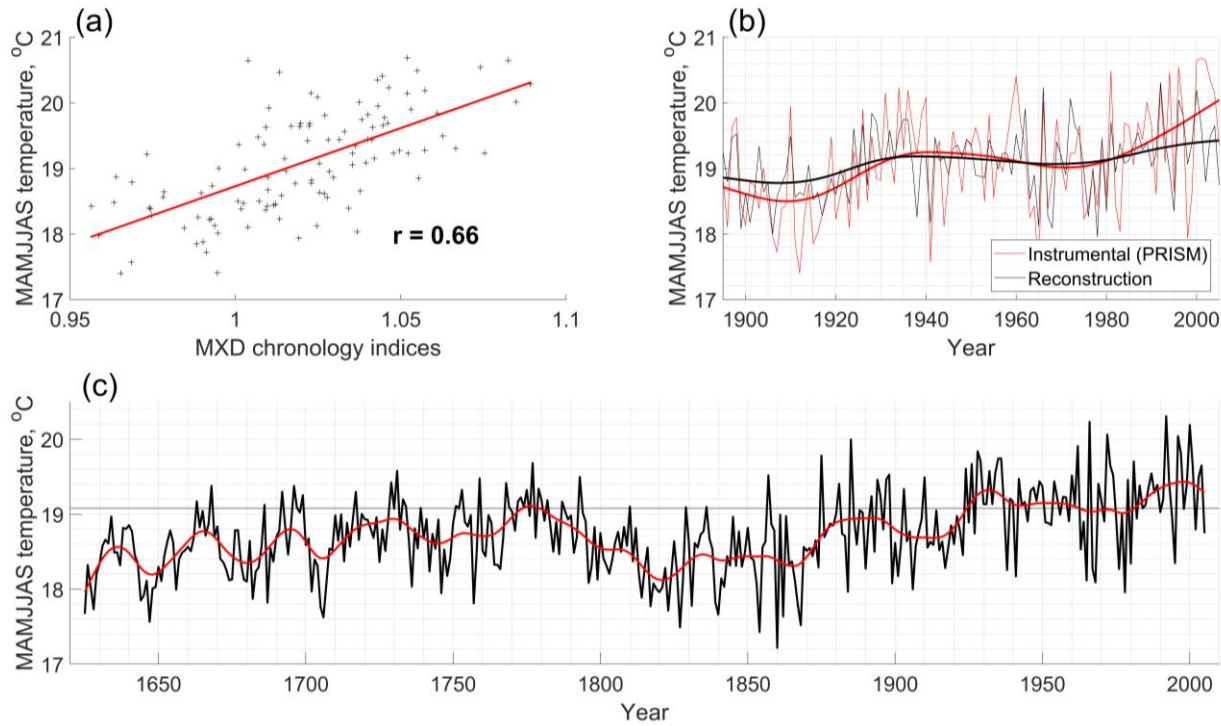
205 **for the target season is indicated with a number. (d) Spatial correlation map (p < 0.10)**
206 **between the MXD chronology and mean March-September (MAMJJAS) temperature**
207 **during 1895-2005 (PRISM data). The map was generated using the KNMI explorer (Trouet**
208 **& Van Oldenborgh, 2013). Sampling location is marked with a dot.**

209   3.2 Reconstruction potential

210 A split-period calibration and validation test shows that the MXD chronology carries a robust
211 signal that can be used for reconstruction of mean MAMJJAS surface temperature (Table S1 in
212 Supporting Information S1). The reconstruction explains 43 % of the variance in instrumental
213 MAMJJAS temperature (Figure 3a, b). Positive RE and CE values on both validation periods
214 (RE = 0.45, CE = 0.27 for 1950-2005, and RE = 0.51, CE = 0.32 for 1895-1949) indicate a good
215 reconstruction potential.

216 MXD indices and the MAMJJAS mean temperature are generally in a good linear dependence
217 (Figure 3a), which supports the use of a linear regression model for the reconstruction. Good
218 agreement between the MXD chronology and the instrumental temperature data on the inter-
219 annual and decadal time scale also supports the reconstruction potential of the tree-ring data
220 (Figure 3b). At decadal scale (obtained with cubic smoothing splines, 50% variance cut-off at
221 50-years period) we see that the tree-ring data follow the temperature variations, with an increase
222 in early 20th century until the 1940's, after which a decrease is observed that re-inflects from the
223 1980's onward. The amplitude of the reconstructed values is lower than that of the instrumental
224 ones by the square root of unexplained variance due to the application of the linear regression
225 method (Esper et al., 2003).

226 Our American Southwest warm-season temperature reconstruction shows that the most recent
227 two decades (1996-2005) are the warmest since 1625 CE (Figure 3c). Our reconstruction shows
228 cold temperatures during the Little Ice Age that are interrupted by a relatively warm period in the
229 late 18th century (1770-1780 CE). After this short period, there is a rapid cooling in the first half
230 of the 19th century followed by a gradual increase for the rest of the 19th century and throughout
231 the 20th century. The coldest 20-year period observed in our reconstruction is centered around
232 1823 CE, and the coldest single year is observed in 1860 CE.

233

Figure 3. X-ray CT based March-September (MAMJJAS) temperature reconstruction. (a) Scatterplot between mean MAMJJAS temperature and MXD chronology indices. (b) Mean MAMJJAS temperature reconstruction over the instrumental period (1895-2005 CE) (red) and the PRISM temperature data (black). Fifty-year smoothing splines show agreement in the 20th century. (C) Mean MAMJJAS temperature reconstruction for the American Southwest over the 1600-2005 CE period (black), a 25-year smoothing spline is shown in red. The horizontal line reflects the average of the reconstructed values for the 1901-2000 CE period.

4 Discussion and Conclusions

4.1 The superiority of MXD as a temperature proxy

Our warm-season temperature reconstruction for the American Southwest is the first X-ray CT based MXD temperature reconstruction. We found that PILO MXD correlates significantly with a wide seven-month warm-season temperature window (Figure 2c), as was also observed in MXD series of other lower latitude sites (Björklund et al., 2017), but contrasts the typically narrow seasonal windows at high-latitude sites (Björklund et al., 2017). Tree-ring records are most frequently studied in the extratropical latitudes (40°-90°) (Anchukaitis et al., 2017, Zhao et al., 2019). The prevailing TRW-based paradigm of tree and site selection (Frank et al., 2022; Fritts et al., 1965; St. George, 2014; Wilson et al., 2021) dictates that at lower latitude sites, moisture availability is the dominant limiting factor for tree growth and trees are predominantly sensitive to moisture availability. Lower latitude tree-ring collections are thus predominantly used for hydroclimate reconstructions (Belmecheri et al., 2016). However, sampling of high-elevation sites in these regions increases the strength of the temperature signal (Kipfmueller & Salzer, 2010), which is even more explicitly the case for MXD data (Trouet et al. 2012, Klippel et al. 2019, Buntgen et

257 al 2010) and confirmed in our study (Figure 2c). MXD RBAR values (Figure 2b) are rather low
258 compared to TRW-based RBAR values from PILO (Salzer, Larson, et al., 2014), which is also
259 observed in other studies, e.g. MXD records from the European Alps (Lopez-Saez et al. 2022,
260 Carrer et al. 2016) or blue intensity records in the Southern Rocky Mountains (Bjorklund et al.
261 2019, Heeter et al. 2020). This is probably due to its lower autocorrelation compared to TRW.

262 Earlier claims have been made that five-needle conifers, such as PILO, are not suitable for X-ray
263 densitometry due to (i) invariability of the latewood as well as (ii) the small rings hindering the
264 standard procedures (Schweingruber 1993). Both claims are disputed in our study showing a
265 strong sensitivity of PILO MXD values to warm-season temperature. The strong MXD
266 temperature signal (Figure 3a) (r = 0.66) may be further fine-tuned with high-resolution
267 anatomical X-ray CT scanning (Van den Bulcke et al. 2019) or through traditional quantitative
268 wood anatomy (Björklund et al., 2023; Lopez-Saez et al., 2023), however at the cost of
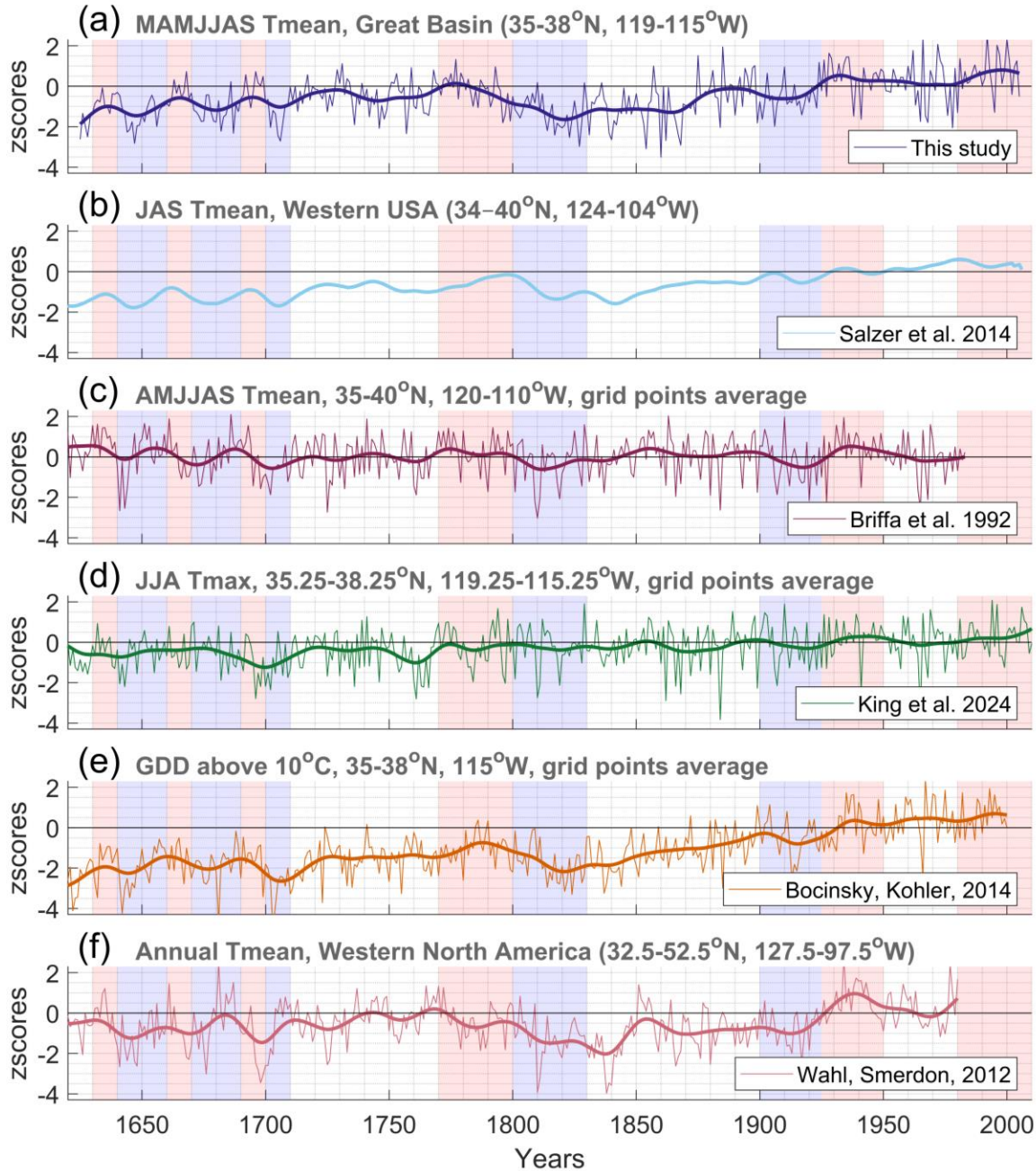269 significantly lower throughput.

270 PILO MXD correlates most strongly with inter-annual temperature variability during those
271 months when cell rehydration and expansion start (April) until cell maturation is completed in
272 September (Ziaco et al., 2016) and thus to the PILO growing season. The correlation gap in July
273 (Figure 2c) is also known as the midsummer decline (Björklund et al., 2017) has been observed
274 in other species and regions and is more pronounced at lower latitudes. This can be due to July
275 being an intermediate period in the middle of the warm season, with less probability of being
276 affected by lower temperatures, thus not necessarily limiting tree growth (Stine & Huybers,
277 2017).

278 4.2 An X-ray CT warm-season temperature reconstruction (1625-2005 CE)

279 Our warm-season temperature reconstruction for the American Southwest (Figure 3c) is one of
280 only a handful of temperature reconstructions for the western part of the USA (Bocinsky &
281 Kohler, 2014; Briffa et al., 1992; King et al., 2024; Salzer et al., 2014b; Wahl & Smerdon, 2012).
282 In contrast to a previous reconstruction based on TRW from the same PILO sites (Figure 4b), our
283 MXD-based temperature reconstruction preserves inter-annual variability. On a lower frequency
284 scale, our reconstruction matches well with the PILO TRW-based reconstruction (Salzer et al.
285 2014), which signifies the presence of a low-frequency variability in our MXD-based
286 reconstruction.

287 Like other regional temperature or temperature-related reconstructions (Figure 4), our
288 reconstruction shows a clear recent warming, as well as a distinct warming phase at the end of
289 the 18th century, which co-occurs with a period of increased solar activity (Figure S4 in
290 Supporting Information S1, (SILSO World Data Center, n.d.)). This late 18th century warming
291 interrupts a relatively cool Little Ice Age, with its coolest period in the early 19th century, when
292 the Dalton solar minimum coincided with a series of large volcanic eruptions (Raible et al.,
293 2016; Sigl et al., 2015). The warming period at the end of the 18th century, as well as the recent
294 warming, is also visible in other regional and continental temperature reconstructions (Figure 4).
295 Some of the considered reconstructions are quite similar to the reconstruction from this study in
296 terms of decadal (Figure 4c) (Briffa et al., 1992), centennial (Figure 4 b,f) (Wahl & Smerdon,
297 2012; Salzer et al.,2014), or both decadal and centennial (Figure 4e) (Bocinsky & Kohler, 2014)
298 variability, while some (King et al., 2024) differ considerably (Figure 4 d). This may be

299 explained by different target climate variable for the reconstruction. Interestingly, the growth
300 degree days reconstruction from Nevada (Figure 4e) (Bocinsky & Kohler, 2014), which is very
301 similar to the reconstruction from this study (Figure 3a), is logically linked by the target climate
302 variable: growth degree days higher than 10 °C should be closely related to the average March -
303 September temperatures. The reconstruction of Bocinsky & Kohler (2014) has also used tree-
304 ring chronologies as predictors, although the data used is completely independent form our
305 study. Many low-frequency variations of our reconstruction from 1700 onwards closely covary
306 with hemispheric and especially continental-scale temperature variability (Figure S4 in
307 Supporting Information S1).

308

Figure 4. Regional temperature reconstructions from the American West. (a) Our X-ray CT MXD-based MAMJJAS mean temperature reconstruction. (b) Decadal TRW-based JAS temperature reconstruction (Salzer et al., 2014a) for the Great Basin (USA), based on PILO high-elevation tree-ring collections. (c) AMJJAS air temperature averaged for four nearest gridpoints of the gridded reconstruction (Briffa et al., 1992). (d) JJA maximum temperature reconstruction (King et al., 2024) averaged for the corresponding region. (e) Growing season growing-degree days (GDD) above 10°C reconstruction (Bocinsky & Kohler, 2014), averaged for three 1 degree squares of the spatial reconstruction. (f) Annual mean temperature reconstruction for Western North America (Wahl & Smerdon, 2012). 30-yrs splines highlight lower frequency variations. Decadal fluctuations of our reconstruction above or below long-term trends that also correspond to other considered reconstructions are highlighted by pink and blue shading respectively.

Given the longevity of PILO and its potential to develop multi-millennia long tree-ring chronologies, the strong temperature signal we found in PILO MXD, as well as the large spatial extent of that signal, provide a strong proof of concept for the successful development of an unprecedented multi-millennial and annual-resolution assessment of past temperature variability in the American Southwest. Furthermore, this new X-ray CT approach for measuring MXD in long-lived and slow-growing trees could be expanded to other regions worldwide that host long-lived, ring-forming species that have a limited temperature signal in their TRW. Examples of such tree species include Rocky Mountains Bristlecone Pine (*Pinus aristata*) in the American Southwest (Salzer & Kipfmueller, 2005; Tintor & Woodhouse, 2021), foxtail pine (*Pinus balfouriana*) (Graumlich, 1993) from the Sierra Nevada, Alerce (*Fitzroya cupressoides*) (Boninsegna & Holmes, 1985) in southern South America, Kauri (*Agathis australis*) in New Zealand (Boswijk et al., 2014), as well as Qillian juniper (*Juniperus przewalskii*) on the Tibetan Plateau (Yang et al., 2014).

Acknowledgments

Data availability statement

The raw MXD measurements, the chronology, as well as the temperature reconstruction, and the files used to generate the Figures are available online (De Mil et al., 2024) via this Figshare link https://figshare.com/s/22b944ba54b1e85073e8

350   . The raw MXD measurements, the chronology, and the temperature reconstruction will be also
351   uploaded upon publication to the Paleoclimatology database of the National Centers for
352   Environmental Information, the National Oceanic and Atmospheric Administration.
353
354   **References**

355   Ahmed, M., Anchukaitis, K. J., Asrat, A., Borgaonkar, H. P., Braida, M., Buckley, B. M., et al.
356   (2013). Continental-scale temperature variability during the past two millennia. *Nature
357   Geoscience*, *6*(5), 339–346. https://doi.org/10.1038/ngeo1797

358   Alfaro-Sánchez, R., Nguyen, H., Klesse, S., Hudson, A., Belmecheri, S., Köse, N., et al. (2018).
359   Climatic and volcanic forcing of tropical belt northern boundary over the past 800 years.
360   *Nature Geoscience*, *11*(12), 933–938. https://doi.org/10.1038/s41561-018-0242-1

361   Anchukaitis, K. J., Wilson, R., Briffa, K. R., Büntgen, U., Cook, E. R., D'Arrigo, R., et al.
362   (2017). Last millennium Northern Hemisphere summer temperatures from tree rings: Part
363   II, spatially resolved reconstructions. *Quaternary Science Reviews*, *163*, 1–22.
364   https://doi.org/10.1016/j.quascirev.2017.02.020

365   Björklund, J., von Arx, G., Nievergelt, D., Wilson, R., Van den Bulcke, J., Günther, B., et al.
366   (2019). Scientific Merits and Analytical Challenges of Tree-Ring Densitometry. *Reviews of
367   Geophysics*, *57*(4), 1224–1264. https://doi.org/10.1029/2019RG000642

368   Björklund, Jesper, Seftigen, K., Schweingruber, F., Fonti, P., Von Arx, G., Bryukhanova, M. V.,
369   et al. (2017). Cell size and wall dimensions drive distinct variability of earlywood and
370   latewood density in Northern Hemisphere conifers. *New Phytologist*, *216*(3), 728–740.
371   https://doi.org/10.1111/nph.14639

372   Björklund, Jesper, Seftigen, K., Stoffel, M., Fonti, M. V., Kottlow, S., Frank, D. C., et al. (2023).
373   Fennoscandian tree-ring anatomy shows a warmer modern than medieval climate. *Nature*,
374   *620*(7972), 97–103. https://doi.org/10.1038/s41586-023-06176-4

375   Bocinsky, R. K., & Kohler, T. A. (2014). A 2,000-year reconstruction of the rain-fed maize
376   agricultural niche in the US Southwest. *Nature Communications*, *5*.
377   https://doi.org/10.1038/ncomms6618

378   Boninsegna, J. A., & Holmes, R. L. (1985). Fitzroya cupressoides yields 1534-year long South
379   American chronology. *Tree Ring Bulletin*, *45*, 37–42.

380   Boswijk, G., Fowler, A. M., Palmer, J. G., Fenwick, P., Hogg, A., Lorrey, A., & Wunder, J.
381   (2014). The late Holocene kauri chronology: Assessing the potential of a 4500-year record
382   for palaeoclimate reconstruction. *Quaternary Science Reviews*, *90*, 128–142.
383   https://doi.org/10.1016/j.quascirev.2014.02.022

384   Briffa, K. R., Jones, P. D., & Schweingruber, F. H. (1992). Tree-Ring Density Reconstructions
385   of Summer Temperature Patterns across Western North America since 1600. *Journal of
386   Climate*. https://doi.org/10.1175/1520-0442(1992)005<0735:trdros>2.0.co;2

387   Briffa, Keith R., Jones, P. D., & Schweingruber, F. H. (1988). Summer temperature patterns over
388   Europe: A reconstruction from 1750 A.D. based on maximum latewood density indices of
389   conifers. *Quaternary Research*, *30*(1), 36–52. https://doi.org/10.1016/0033-5894(88)90086-

390   5

391   Bruening, J. M., Tran, T. J., Bunn, A. G., Weiss, S. B., & Salzer, M. W. (2017). Fine-scale
392   modeling of bristlecone pine treeline position in the Great Basin, USA. *Environmental*
393   *Research Letters*, *12*(1). https://doi.org/10.1088/1748-9326/aa5432

394   Van den Bulcke, J., Wernersson, E. L. G., Dierick, M., Van Loo, D., Masschaele, B., Brabant,
395   L., et al. (2014). 3D tree-ring analysis using helical X-ray tomography. *Dendrochronologia*,
396   *32*(1), 39–46. https://doi.org/10.1016/j.dendro.2013.07.001

397   Bunn, A. G. (2008). A dendrochronology program library in R (dplR). *Dendrochronologia*,
398   *26*(2), 115–124. https://doi.org/10.1016/j.dendro.2008.01.002

399   Bunn, A. G. (2010). Statistical and visual crossdating in R using the dplR library.
400   *Dendrochronologia*, *28*(4), 251–258. https://doi.org/10.1016/j.dendro.2009.12.001

401   Bunn, A. G., Hughes, M. K., & Salzer, M. W. (2011). Topographically modified tree-ring
402   chronologies as a potential means to improve paleoclimate inference: A letter. *Climatic*
403   *Change*, *105*(3–4), 627–634. https://doi.org/10.1007/s10584-010-0005-5

404   Büntgen, U., Frank, D., Trouet, V., & Esper, J. (2010). Diverse climate sensitivity of
405   Mediterranean tree-ring width and density. *Trees - Structure and Function*, *24*(2), 261–273.
406   https://doi.org/10.1007/s00468-009-0396-y

407   Bytebier, J., De Mil, T., Vanhellemont, M., Verheyen, K., Haneca, K., & Van den Bulcke, J.
408   (2022). Linking wood density records of common beech (Fagus sylvatica L.) with
409   temperature and precipitation variability from a temperate lowland site.
410   *Dendrochronologia*, *76*, 126018.
411   https://doi.org/https://doi.org/10.1016/j.dendro.2022.126018

412   Cayan, D. R., Redmond, K. T., & Riddle, L. G. (1999). ENSO and hydrologic extremes in the
413   western United States. *Journal of Climate*, *12*(9), 2881–2893. https://doi.org/10.1175/1520-
414   0442(1999)012<2881:EAHEIT>2.0.CO;2

415   Cook, E. R., Woodhouse, C. A., Eakin, C. M., Meko, D. H., & Stahle, D. W. (2004). Long-term
416   aridity changes in the western United States. *Science*, *306*(5698), 1015–1018.
417   https://doi.org/10.1126/science.1102586

418   Daly, C., Halbleib, M., Smith, J. I., Gibson, W. P., Doggett, M. K., Taylor, G. H., et al. (2008).
419   Physiographically sensitive mapping of climatological temperature and precipitation across
420   the conterminous United States. *International Journal of Climatology*, *28*(15), 2031–2064.
421   https://doi.org/10.1002/joc.1688

422   Emile-Geay, J., McKay, N. P., Kaufman, D. S., von Gunten, L., Wang, J., Anchukaitis, K. J., et
423   al. (2017). A global multiproxy database for temperature reconstructions of the Common
424   Era. *Scientific Data*, *4*(1), 170088. https://doi.org/10.1038/sdata.2017.88

425   Esper, J. ;, Cook, E. R. ;, Krusic, P. J. ;, Peters, K. ;, Schweingruber, F. H., Citation Esper, J., et
426   al. (2003). *Tests of the RCS Method for Preserving Low-Frequency Variability in Long*
427   *Tree-Ring Chronologies Item Type Article*. Retrieved from
428   http://hdl.handle.net/10150/262573

429 Esper, J., Frank, D. C., Timonen, M., Zorita, E., Wilson, R. J. S., Luterbacher, J., et al. (2012).
430   Orbital forcing of tree-ring data. *Nature Climate Change*, *2*(12), 862–866.
431   https://doi.org/10.1038/nclimate1589

432 Esper, J., George, S. S., Anchukaitis, K., D'Arrigo, R., Ljungqvist, F. C., Luterbacher, J., et al.
433   (2018, August 1). Large-scale, millennial-length temperature reconstructions from tree-
434   rings. *Dendrochronologia*. Elsevier GmbH. https://doi.org/10.1016/j.dendro.2018.06.001

435 Ferguson, C. W. (1968). Bristlecone pine: Science and esthetics. *Science*, *159*(3817), 839–846.
436   https://doi.org/10.1126/science.159.3817.839

437 Frank, D., Fang, K., & Fonti, P. (2022). Dendrochronology: Fundamentals and Innovations. In R.
438   T. W. Siegwolf, J. R. Brooks, J. Roden, & M. Saurer (Eds.), *Stable Isotopes in Tree Rings:*
439   *Inferring Physiological, Climatic and Environmental Responses* (pp. 21–59). Cham:
440   Springer International Publishing. https://doi.org/10.1007/978-3-030-92698-4_2

441 Fritts, H., Smith, D., Cardis, J., & Budelsky, C. (1965). Tree-Ring Characteristics Along a
442   Vegetation Gradient in Northern Arizona, *46*(4), 394–401.

443 St. George, S. (2014). An overview of tree-ring width records across the Northern Hemisphere.
444   *Quaternary Science Reviews*, *95*(July 2014), 132–150.
445   https://doi.org/10.1016/j.quascirev.2014.04.029

446 St. George, S., & Esper, J. (2019). Concord and discord among Northern Hemisphere
447   paleotemperature reconstructions from tree rings. *Quaternary Science Reviews*, *203*(xxxx),
448   278–281. https://doi.org/10.1016/j.quascirev.2018.11.013

449 Graumlich, L. J. (1993). A 1000-Year Record of Temperature and Precipitation in the Sierra
450   Nevada. *Quaternary Research*. https://doi.org/10.1006/qres.1993.1029

451 Holmes., R. L. (1983). Computer-assisted quality control in tree-ring dating and measurement.
452   *Tree-Ring Bulletin*.

453 King, K. E., Cook, E. R., Anchukaitis, K. J., Cook, B. I., Smerdon, J. E., Seager, R., et al. (2024).
454   Increasing prevalence of hot drought across western North America since the 16th century,
455   *4289*(January), 1–10. https://doi.org/10.1126/sciadv.adj4289

456 Kipfmueller, K. F., & Salzer, M. W. (2010). Linear trend and climate response of five-needle
457   pines in the western United States related to treeline proximity. *Canadian Journal of Forest*
458   *Research*, *40*(1), 134–142. https://doi.org/10.1139/X09-187

459 Klippel, L., Büntgen, U., Konter, O., Kyncl, T., & Esper, J. (2020). Climate sensitivity of high-
460   and low-elevation Larix decidua MXD chronologies from the Tatra Mountains.
461   *Dendrochronologia*, *60*(July 2019), 1–9. https://doi.org/10.1016/j.dendro.2020.125674

462 LaMarche, V. C., & Stockton, C. W. (1974). Chronologies from temperature-sensitive
463   bristlecone pines at upper treeline in western United States. *Tree-Ring Bulletin*, *34*, 21–45.

464 Lopez-Saez, J., Corona, C., von Arx, G., Fonti, P., Slamova, L., & Stoffel, M. (2023). Tree-ring
465   anatomy of Pinus cembra trees opens new avenues for climate reconstructions in the
466   European Alps. *Science of the Total Environment*, *855*.
467   https://doi.org/10.1016/j.scitotenv.2022.158605

468 Meko, D. M., Touchan, R., & Anchukaitis, K. J. (2011). Seascorr: A MATLAB program for
469   identifying the seasonal climate signal in an annual tree-ring time series. *Computers and*
470   *Geosciences*, *37*(9), 1234–1241. https://doi.org/10.1016/j.cageo.2011.01.013

471 Melvin, T. M., & Briffa, K. R. (2008). A "signal-free" approach to dendroclimatic
472   standardisation. *Dendrochronologia*, *26*(2), 71–86.
473   https://doi.org/10.1016/j.dendro.2007.12.001

474 De Mil, T., & Van den Bulcke, J. (2023). Tree Core Analysis with X-ray Computed
475   Tomography. *Journal of Visualized Experiments : JoVE*, (199), 1–28.
476   https://doi.org/10.3791/65208

477 De Mil, T., Vannoppen, A., Beeckman, H., Van Acker, J., & Van Den Bulcke, J. (2016). A field-
478   to-desktop toolchain for X-ray CT densitometry enables tree ring analysis. *Annals of*
479   *Botany*, *117*(7), 1187–1196. https://doi.org/10.1093/aob/mcw063

480 De Mil, T., Meko, M., Belmecheri, S., February, E., Therrell, M., Van den Bulcke, J., & Trouet,
481   V. (2021). A lonely dot on the map: Exploring the climate signal in tree-ring density and
482   stable isotopes of clanwilliam cedar, South Africa. *Dendrochronologia*, *69*(August).
483   https://doi.org/10.1016/j.dendro.2021.125879

484 De Mil, T., Matskovsky, V., Salzer, M. W., Corluy, L., Verschuren, L., Pearson, C. et al. (2024).
485   Bristlecone Pine Maximum Latewood Density from the California White Mountains and
486   March-to-September Temperature Reconstruction for American Southwest [Dataset].
487   Figshare. https://doi.org/10.6084/m9.figshare.25562499.v1

488 Raible, C. C., Brönnimann, S., Auchmann, R., Brohan, P., Frölicher, T. L., Graf, H. F., et al.
489   (2016). Tambora 1815 as a test case for high impact volcanic eruptions: Earth system
490   effects. *Wiley Interdisciplinary Reviews: Climate Change*, *7*(4), 569–589.
491   https://doi.org/10.1002/wcc.407

492 Rathgeber, C. B. K. (2017). Conifer tree-ring density interannual variability - anatomical,
493   physiological and environmental determinants. *New Phytologist*, *216*(3), 621–625.
494   https://doi.org/10.1111/NPH.14763

495 De Ridder, M., Van Den Bulcke, J., Vansteenkiste, D., Van Loo, D., Dierick, M., Masschaele,
496   B., et al. (2011). High-resolution proxies for wood density variations in Terminalia superba.
497   *Annals of Botany*, *107*(2), 293–302. https://doi.org/10.1093/aob/mcq224

498 Salzer, M. W., & Kipfmueller, K. F. (2005). Reconstructed temperature and precipitation on a
499   millennial timescale from tree-rings in the southern Colorado Plateau, U.S.A. *Climatic*
500   *Change*, *70*(3), 465–487. https://doi.org/10.1007/s10584-005-5922-3

501 Salzer, M. W., Hughes, M. K., Bunn, A. G., & Kipfmueller, K. F. (2009). Recent unprecedented
502   tree-ring growth in bristlecone pine at the highest elevations and possible causes.
503   *Proceedings of the National Academy of Sciences of the United States of America*, *106*(48),
504   20348–20353. https://doi.org/10.1073/pnas.0903029106

505 Salzer, M. W., Larson, E. R., Bunn, A. G., & Hughes, M. K. (2014). Changing climate response
506   in near-treeline bristlecone pine with elevation and aspect. *Environmental Research Letters*,
507   *9*(11). https://doi.org/10.1088/1748-9326/9/11/114007

508   Salzer, M. W., Bunn, A. G., Graham, N. E., & Hughes, M. K. (2014a). Five Millennia of
509   Paleotemperature from Tree- Rings in the Great Basin , USA.
510   https://doi.org/10.1007/s00382-013-1911-9

511   Salzer, M. W., Bunn, A. G., Graham, N. E., & Hughes, M. K. (2014b). Five millennia of
512   paleotemperature from tree-rings in the Great Basin, USA. *Climate Dynamics*, *42*(5–6),
513   1517–1526. https://doi.org/10.1007/s00382-013-1911-9

514   Salzer, M. W., Pearson, C. L., & Baisan, C. H. (2019). Dating the methuselah walk bristlecone
515   pine floating chronologies. *Tree-Ring Research*, *75*(1), 61–66. https://doi.org/10.3959/1536-
516   1098-75.1.61

517   Schweingruber, F., Fritts, H., Braker, O., Drew, L., & Schar, E. (1978). The Xray technique as
518   applied to dendroclimatology. *Tree-Ring Bulletin*, *38*, 61–91.

519   Sigl, M., Winstrup, M., McConnell, J. R., Welten, K. C., Plunkett, G., Ludlow, F., et al. (2015).
520   Timing and climate forcing of volcanic eruptions for the past 2,500 years. *Nature*,
521   *523*(7562), 543–549. https://doi.org/10.1038/nature14565

522   SILSO World Data Center. (n.d.). No Title.

523   Stine, A. R., & Huybers, P. (2017). Implications of Liebig's law of the minimum for tree-ring
524   reconstructions of climate. *Environmental Research Letters*, *12*(11).
525   https://doi.org/10.1088/1748-9326/aa8cd6

526   Tintor, W. L., & Woodhouse, C. A. (2021). The variable climate response of Rocky Mountain
527   bristlecone pine (Pinus aristata Engelm.). *Dendrochronologia*, *68*, 125846.
528   https://doi.org/10.1016/j.dendro.2021.125846

529   Tran, T. J., Bruening, J. M., Bunn, A. G., Salzer, M. W., & Weiss, S. B. (2017). Cluster analysis
530   and topoclimate modeling to examine bristlecone pine tree-ring growth signals in the Great
531   Basin, USA. *Environmental Research Letters*, *12*(1). https://doi.org/10.1088/1748-
532   9326/aa5388

533   Trouet, V., Panayotov, M. P., Ivanova, A., & Frank, D. (2012). A pan-European summer
534   teleconnection mode recorded by a new temperature reconstruction from the northeastern
535   Mediterranean (ad 1768-2008). *Holocene*, *22*(8), 887–898.
536   https://doi.org/10.1177/0959683611434225

537   Trouet, V., Diaz, H. F., Wahl, E. R., Viau, A. E., Graham, R., Graham, N., & Cook, E. R. (2013).
538   A 1500-year reconstruction of annual mean temperature for temperate North America on
539   decadal-to-multidecadal time scales. *Environmental Research Letters*, *8*(2).
540   https://doi.org/10.1088/1748-9326/8/2/024008

541   Trouet, Valerie, & Van Oldenborgh, G. J. (2013). KNMI climate explorer: A web-based research
542   tool for high-resolution paleoclimatology. *Tree-Ring Research*, *69*(1), 3–13.
543   https://doi.org/10.3959/1536-1098-69.1.3

544   Vlassenbroeck, J., Dierick, M., Masschaele, B., Cnudde, V., Van Hoorebeke, L., & Jacobs, P.
545   (2007). Software tools for quantification of X-ray microtomography at the UGCT. *Nuclear
546   Instruments and Methods in Physics Research, Section A: Accelerators, Spectrometers,
547   Detectors and Associated Equipment*, *580*(1 SPEC. ISS.), 442–445.

548   https://doi.org/10.1016/j.nima.2007.05.073

549 Wahl, E. R., & Smerdon, J. E. (2012). Comparative performance of paleoclimate field and index
550   reconstructions derived from climate proxies and noise-only predictors. *Geophysical*
551   *Research Letters*, *39*(6), 1–5. https://doi.org/10.1029/2012GL051086

552 Wahl, E. R., Zorita, E., Diaz, H. F., & Hoell, A. (2022). Southwestern United States drought of
553   the 21st century presages drier conditions into the future. *Communications Earth and*
554   *Environment*, *3*(1), 1–14. https://doi.org/10.1038/s43247-022-00532-4

555 Wigley, T. M. L., Briffa, K. R., & Jones, P. D. (1984). On the average value of correlated time
556   series with applications in dendroclimatology and hydrometeorology. *Journal of Climate &*
557   *Applied Meteorology*, *23*(2), 201–213. https://doi.org/10.1175/1520-
558   0450(1984)023<0201:OTAVOC>2.0.CO;2

559 Williams, A. P., Cook, E. R., Smerdon, J. E., Cook, B. I., Abatzoglou, J. T., Bolles, K., et al.
560   (2020). Erratum: Large contribution from anthropogenic warming to an emerging North
561   American megadrought (American Association for the Advancement of Science (2020)
562   DOI: 10.1126/science.aaz9600). *Science*, *370*(6516), 314–318.
563   https://doi.org/10.1126/SCIENCE.ABF3676

564 Wilson, R., Allen, K., Baker, P., Boswijk, G., Buckley, B., Cook, E., et al. (2021). Evaluating the
565   dendroclimatological potential of blue intensity on multiple conifer species from Tasmania
566   and New Zealand. *Biogeosciences*, *18*(24), 6393–6421. https://doi.org/10.5194/bg-18-6393-
567   2021

568 Yang, B., Qin, C., Wang, J., He, M., Melvin, T. M., Osborn, T. J., & Briffa, K. R. (2014). A
569   3,500-year tree-ring record of annual precipitation on the northeastern Tibetan Plateau.
570   *Proceedings of the National Academy of Sciences of the United States of America*, *111*(8),
571   2903–2908. https://doi.org/10.1073/pnas.1319238111

572 Zang, C., & Biondi, F. (2015). Treeclim: An R package for the numerical calibration of proxy-
573   climate relationships. *Ecography*, *38*(4), 431–436. https://doi.org/10.1111/ecog.01335

574 Zhao, S., Pederson, N., D'Orangeville, L., HilleRisLambers, J., Boose, E., Penone, C., et al.
575   (2019). The International Tree-Ring Data Bank (ITRDB) revisited: Data availability and
576   global ecological representativity. *Journal of Biogeography*, *46*(2), 355–368.
577   https://doi.org/10.1111/jbi.13488

578 Ziaco, E., Biondi, F., Rossi, S., & Deslauriers, A. (2016). Environmental drivers of cambial
579   phenology in Great Basin bristlecone pine. *Tree Physiology*, *36*(7), 818–831.
580   https://doi.org/10.1093/treephys/tpw006

581
582